Global and Planetary Change 172 (2019) 454–463

Contents lists available at ScienceDirect

Global and Planetary Change

journal homepage: www.elsevier.com/locate/gloplacha

Research article

Coastal Sea level rise around the China Seas

Ying Qu[a,b], Svetlana Jevrejeva[b], Luke P. Jackson[c], John C. Moore[a,d,e,*]

[a] College of Global Change and Earth System Science, Beijing Normal University, Beijing, China
[b] National Oceanography Center, 6 Brownlow Street, Liverpool L3 5DA, UK
[c] Programme for Economic Modelling, Nuffield College, 1 New Road, Oxford University, OX1 1NF, UK
[d] Arctic Centre, University of Lapland, P.O. Box 122, 96101 Rovaniemi, Finland
[e] CAS Center for Excellence in Tibetan Plateau Earth Sciences, Beijing 100101, China

ARTICLE INFO

Keywords:
Sea level rise
China
Tide gauge records
Vertical land motion
Sea level budget
Sea level projections

ABSTRACT

We analyze the sea level rise along the Bohai Sea, the Yellow Sea, the East China Sea, and the South China Sea (the "China Seas") coastline using 25 tide gauge records beginning with Macau in 1925, but with most starting during the 1950s and 60s. The main problem in estimating sea level rise for the period is the lack of vertical land movement (VLM) data for the tide gauge stations. We estimated VLM using satellite altimetry covering the 18 stations with records spanning 1993–2016. The results show that many tide gauge stations, typically in cities, have undergone significant subsidence due to groundwater extraction. After removing the VLM from tide gauge records, the 1993–2016 sea level rise rate is 3.2 ± 1.1 mm/yr, and 2.9 ± 0.8 mm/yr over the longer 1980–2016 period. We estimate the steric sea level contribution to be up to 0.9 ± 0.3 mm/yr, and contributions from ice mass loss from glaciers and ice sheets of up to 1.1 ± 0.1 mm/yr over the last 60 years. Contributions from VLM range between −4.5 ± 1.0 mm/yr and 1.4 ± 1.3 mm/yr across the stations. Projections of coastal sea level probability distributions under future climate scenarios show that the steric factor is the main contributor under both the RCP 4.5 and High-end RCP 8.5 scenarios except in the upper tails under High-end RCP 8.5 when the Antarctic ice sheet makes the greatest contribution. By 2100 we expect median coastal sea level rises at the stations of 48–61 cm under RCP 4.5, and 84–99 cm under High-end RCP 8.5 scenario.

1. Introduction

Reliable estimates of future sea levels are of vital importance for low lying coastal areas subject to gradual encroachment and flooding (e.g. Rowley et al., 2007; Hallegatte et al., 2013; Kopp et al., 2014; Jackson and Jevrejeva, 2016). Coastal inundation is the product of many factors including the local vertical land-motion, ocean dynamics and expansion, along with changes in terrestrial ice masses. Coastal rises are expected to be much greater than mean ocean basin sea levels (Church et al., 2013; Jevrejeva et al., 2016).

Like many coastlines, China and the countries around the China Seas, (that is the Bohai Sea, the Yellow Sea, the East China Sea, and the South China Sea, Fig. 1) have a larger population and a greater concentration of infrastructure and capital investment at or close to the coastline than the country average. The close proximity of assets to the coast places them in a potentially vulnerable position regarding rising sea levels (Han et al., 1995; Chen, 1997; Shi et al., 2000; Wu et al., 2003; Wang et al., 2012). The "China Sea Level Bulletin of 2016 (2017)" (www.soa.gov.cn/zwgk/hygb) reported Chinese coastal sea levels increased by 3.2 mm/yr from 1980 to 2016 according to tide gauge records, as the bulletin estimated the rate without uncertainties, in our analysis we will verify the rate. In 2016 Chinese sea levels were 82 mm higher than the 1993–2011 mean. The East China Sea experienced the largest increases.

Tide gauges provide long-term records of sea level change. Emery and Yu (1981) reported an average rate of about 2.5 mm/yr over the 1950s to 1980s from eight tide gauge stations. Chen (1991) used long records from two tide gauge stations in Shanghai to show seas rising by 1.0 mm/yr from 1922 to 1987 after accounting for local tectonic movement, ground subsidence and river discharge, which had been neglected in previous studies. Tectonic subsidence accounted for, at most, 1/3 of the relative sea level rise. Ren (1993) studied the sea level changes in China over the past 80 years using monthly records from 32 tide gauge stations, (28 on the Chinese mainland and four in Taiwan); 20 stations showed rises while the other 12 stations had falling sea level, with significant spatial variability. Sea level rose faster in deltas and coastal plains largely due to the local subsidence (Chen, 1991; Ren, 1993). Ding et al. (2001) analyzed the Hong Kong tide gauge records

* Corresponding author at: College of Global Change and Earth System Science, Beijing Normal University, Beijing, China.
E-mail address: john.moore.bnu@gmail.com (J.C. Moore).

https://doi.org/10.1016/j.gloplacha.2018.11.005
Received 10 August 2018; Received in revised form 13 November 2018; Accepted 13 November 2018
Available online 15 November 2018

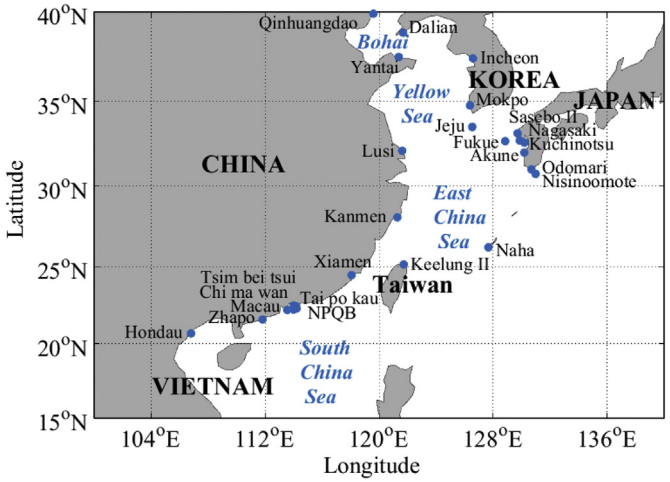

Fig. 1. The spatial distribution of tide gauge stations in study area.

from 1954 to 1999 finding a rising trend of 1.9 ± 0.4 mm/yr. He et al. (2014) used spatial empirical orthogonal function analysis of tide gauge data and satellite altimetry data to reconstruct the sea level change in the Pearl River Delta from 1959 to 2011, finding relative sea level increases of 4.1 mm/yr. Chen et al. (2018) found that tide gauge data show increasing trends of between 1 and 5 mm/yr from mid-20th to 21st century along the Chinese coast. Wang et al. (2016) used the Macau record from 1925 to 2010 and satellite altimetry data to simulate future sea level rise based on CMIP5 climate models under different climate scenarios with the SimCLIM software package (Warrick et al., 2005). Wang et al. (2016) projected rises of 65–118 cm by 2100 under the RCP 8.5 scenario.

In this paper, we use all available tide gauge stations along the China Seas coastline, to study how sea level has changed in the past and determine the relative importance of the different contributors to it. To construct this sea level budget at individual locations, we examine how vertical land movement (VLM) including glacial isostatic adjustment (GIA) and local land-motion, steric effects and present-day mass redistribution due to mass fluxes from glaciers, ice sheets and land-water storage changes, have affected sea level observed by tide gauges. Finally, we project future sea level and its component parts at each tide gauge station for a set of climate scenarios.

2. Data and methods

2.1. Study area and tide gauge data

For convenience we denote the "China Seas coast" as the regions located between 100 and 140°E and, 15–40°N, although the coastline is spread over a number of different countries. Monthly tide gauge data come from the Permanent Service for Mean Sea level (PSMSL) (Holgate et al., 2013; PSMSL, 2017). The 25 stations are shown in Fig. 1, 24 stations have records longer than 40 years, 15 are between 50 and 60 years long, and 2 are longer. Chi Ma Wan has the shortest record, only 37 years, and also has the lowest completeness (63%) of the tide gauge records we use (detailed information is in the Supplementary Information). North Point and Quarry Bay in Hong Kong have matching datum information (Ding et al., 2001), so here we merge them into one time series and rename it as NPQB.

The monthly sea level change (SLC) records from each tide gauge are presented in Fig. 2, and the average rates for each station are shown in Table 1. Among all 25 stations, 13 Stations are in China, 3 are in Korea, 8 are in Japan, and 1 is in Vietnam. We estimate sea level trends and the error bar using a simple linear regression model that contains an annual and semi-annual cycle. As the residuals in the linear regression model used to estimate the sea level trends usually contain serial correlation, it will underestimate the true standard error, and so here we assume the residuals follow an autoregressive model of order 1 (AR1), then adjust the standard error by reducing the degree of freedom following Dangendrof et al. (2014). Average rates of sea level change from the stations in the tide gauge records vary from −2.3 ± 1.9 to 5.7 ± 0.4 mm/yr. Of the records that extend past the year 2000, all stations are rising at rates between 0.4 ± 1.2 and 5.7 ± 0.4 mm/yr. Among all 25 stations, Macau is the only one which begins prior to 1950, and from 1925 to 1985 (when it stopped), its sea level rose at the rate of 0.3 ± 0.5 mm/yr.

2.2. Satellite altimetry data and sea level pressure data

As there is no Global Positioning System (GPS) data at tide gauge stations in mainland China to estimate VLM, we made use of the high-resolution monthly satellite altimetry data from AVISO (Archiving, Validation, and Interpretation of Satellite Oceanographic Data) and tide gauge data instead. The satellite altimetry data used for VLM are monthly near-global sea level anomaly data at 0.25° × 0.25°resolution from 1993 to 2016 provided by AVISO. Satellite altimetry measures absolute sea level (ASL) which is relative to a global reference frame and as a result, it is not affected by local VLM. Tide gauge data is relative to a benchmark which is affected by land movement, thus we can estimate the VLM from the difference between ASL measured by satellite altimetry and coastal sea level measured by tide gauges in locations without direct GPS observations (Kuo et al., 2004; Ostanciaux et al., 2012; Chen et al., 2018; Wöppelmann and Marcos, 2016). However, limitations of this method (the difference between altimetry and tide gauges) have been discussed in previously published studies (Kleinherenbrink et al., 2018) and the difference in observations made by satellite altimetry and tide gauges have been discussed in Prandi et al., 2009.

Raw AVISO sea level anomaly data have already been corrected for sea level pressure (SLP) variations. We correct the tide gauge records using six-hourly SLP from NCEP/NCAR Reanalysis datasets (Kalnay et al., 1996).

2.3. Seawater temperature and salinity data

To study the steric sea level contribution we use EN4.2.0 quality controlled ocean temperature and salinity datasets (Good et al., 2013), in which biases from mechanical bathythermograph and expendable bathythermograph profiles were corrected following Gouretski and Reseghetti (2010).

Depth-integrated steric sea level (η_{steric}) can be computed from the density profile over depth, which we derive from gridded potential temperature and salinity data that is available for the whole duration of the tide gauge data. Then, following (Dangendrof et al., 2014):

$$\eta_{steric} = -\frac{1}{\rho_0}\int_{-H}^{0}(\rho - \bar{\rho})dz \quad (1)$$

where ρ_0 is the reference density (1025 kg/m^3) of sea water, ρ is its in situ density computed with the TEOS-10 software (McDougall and Barker, 2011), $\bar{\rho}$ is the time averaged density over the whole record duration, and H is the basin depth below mean sea level.

2.4. Present-day mass redistribution

We use estimates from Frederikse et al. (2018), calculated as the sum of mass losses to the ocean from small ice masses, the Greenland Ice Sheet (GIS) and the Antarctic Ice Sheet (AIS) and terrestrial water storage mass changes over the period 1958–2014. Frederikse et al. (2018) used glacier mass losses from Marzeion et al. (2015); GIS estimates from Kjeldsen et al. (2015) for the period 1958–1992, and the RACMO2.3 surface mass and energy balance model for 1992–2014; AIS

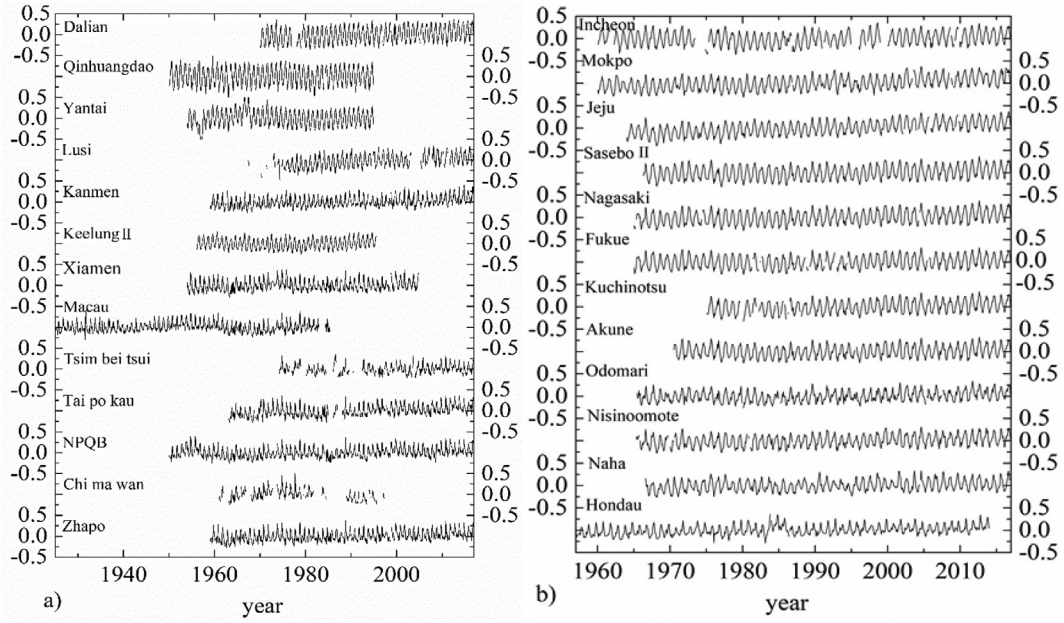

Fig. 2. The monthly sea level change (SLC, Units: m) from all the tide gauge records. Long term means are removed from all series.

Table 1
Tide gauge stations and trends (mm/yr), the confidence interval is at 95% level.

Station name	Time span	SLC rate
Dalian	1970–2016	3.5 ± 0.4
Qinhuangdao	1950–1994	−0.0 ± 0.6
Yantai	1954–1994	−0.2 ± 2.2
Lusi	1967–2016	5.7 ± 0.4
Kanmen	1959–2016	2.4 ± 0.4
Keelung II	1956–1995	0.5 ± 0.8
Xiamen	1954–2004	1.1 ± 0.6
Macau	1925–1985	0.3 ± 0.5
Tsim bei tsui	1974–2016	0.4 ± 1.2
Tai po kau	1963–2016	3.2 ± 0.6
NPQB	1950–2016	1.3 ± 0.5
Chi ma wan	1961–1997	−2.3 ± 1.9
Zhapo	1959–2016	2.3 ± 0.4
Incheon	1960–2016	1.4 ± 0.5
Mokpo	1960–2016	3.9 ± 0.5
Jeju	1964–2016	5.3 ± 0.4
Sasebo II	1966–2016	2.2 ± 0.5
Nagasaki	1965–2016	2.6 ± 0.4
Fukue	1965–2016	1.5 ± 0.4
Kuchinotsu	1975–2016	3.3 ± 0.5
Akune	1970–2016	1.4 ± 0.5
Odomari	1965–2016	2.1 ± 0.5
Nisinoomote	1965–2016	2.3 ± 0.4
Naha	1966–2016	2.2 ± 0.6
Hondau	1957–2013	2.1 ± 0.4

mass balance was also based on RACMO2.3 model outputs; Land-water storage was based on PCR-GLOWB model (Wada et al., 2014). Mass component at tide gauge locations are the combination of contributions from glaciers, GIS and AIS, and are extracted from the "fingerprints" for glaciers and ice sheets (Jackson and Jevrejeva, 2016; Jevrejeva et al., 2016), which were scaled using the contributions from relevant sea level components.

2.5. Probabilistic Sea level projections by 2100

We estimate probabilistic sea level projections for each tide gauge location from regional sea level projections by Jackson and Jevrejeva (2016). We produce estimates of sea level rise for 2010–2100 at each station under the IPCC RCP 4.5 and RCP 8.5 (Moss et al., 2010). We name our RCP 8.5 as "High-end RCP 8.5" following Jackson and Jevrejeva, 2016. The difference between our High-end RCP 8.5 and the IPCC RCP 8.5 scenarios for sea level is that our High-end RCP 8.5 sea level projections are supplemented by Greenland and Antarctic contributions from an expert elicitation by Bamber and Aspinall (2013), which exhibit large uncertainties in the upper tail coming from the AIS and GIS. The West and East Antarctic ice sheets both have particularly high potential rates, presumably due to dynamically driven processes along their extensive marine-based margins (Jevrejeva et al., 2014; Grinsted et al., 2015; Jackson and Jevrejeva, 2016).

With RCP 4.5 and High-end RCP 8.5 we produce projections for sea level components: steric and dynamic sea level, ice mass loss from glaciers and ice sheets in Greenland and Antarctic (Jackson and Jevrejeva, 2016). Contributions from land water storage (Wada et al., 2012) and GIA are scenario independent. To account for GIA, we use the time-integrated spatial field of GIA induced sea level change from the ICE 6G model (Peltier et al., 2015). Following Jackson and Jevrejeva (2016) we use steric and dynamic sea level component from 31 CMIP5 model outputs, Glaciers, GIS and AIS fingerprints from Bamber and Riva (2010), and land water storage from Wada et al. (2012). In this study we have not included projections of the local vertical land movement into the future sea level projections and we discuss uncertainties associated with this in the Discussion section.

3. Sea level trends

3.1. Vertical land motion

VLM is the main source of contamination in tide gauge records globally and is caused by several geophysical processes (Church et al., 2013), including local tectonic changes, subsidence/uplifts from groundwater extraction, earthquakes, and GIA which is related to the solid earth response to the last deglaciation. VLM are estimated as AL (Altimetry) minus TG (Tide gauge) rates. There are 18 tide gauge stations with records covering 1993–2016 matching the satellite altimetry data period. These 18 stations are considered for detailed analysis in our study. Modeled GIA corrections from the ICE-6G_C_VM5a model (Stuhne and Peltier, 2015) are available for each tide gauge location (Table 2). All the 18 stations we consider have GIA uplift rates of 0.10–0.56 mm/yr.

Table 2
SLC trend from tide gauge and satellite altimetry during 1993–2016 (Units: mm/yr), the confidence interval is at 95% level.

	SLC trend from TG[a]	SLC trend from AL[b]	r[c]	VLM trend (AL-TG)	VLM trend from SONEL[d]	GIA[e] rate	LLM[f] rate
Dalian	4.5 ± 0.9	2.8 ± 0.9	0.88	−1.7 ± 0.9	−0.8 ± 0.4	0.44	−2.1 ± 0.9
Lusi	6.8 ± 1.9	3.2 ± 2.1	0.55	−3.6 ± 2.6	−2.6 ± 0.8	0.53	−4.1 ± 2.6
Kanmen	5.0 ± 1.3	3.7 ± 1.3	0.89	−1.3 ± 0.9	−1.3 ± 0.5	0.45	−1.8 ± 0.9
Tsim bei tsui	1.6 ± 2.1	2.6 ± 1.1	0.85	1.0 ± 1.0	0.4 ± 0.6	0.43	0.6 ± 1.0
Tai po kau	2.7 ± 1.5	2.7 ± 1.1	0.94	−0.0 ± 0.8	0.1 ± 0.5	0.41	−0.4 ± 0.6
NPQB	1.8 ± 1.6	2.7 ± 1.2	0.95	0.9 ± 0.7	N/A	0.40	0.5 ± 0.7
Zhapo	2.5 ± 1.3	3.2 ± 1.1	0.93	0.7 ± 0.8	0.8 ± 0.5	0.46	0.2 ± 0.8
Incheon	4.8 ± 3.1	6.2 ± 1.2	0.69	1.4 ± 1.3	2.0 ± 0.6[g]	0.56	0.8 ± 1.3
Mokpo	7.4 ± 1.8	2.9 ± 0.9	0.78	−4.5 ± 1.0	N/A	0.51	−5.0 ± 1.0
Jeju	6.5 ± 0.9	2.9 ± 0.9	0.89	−3.6 ± 0.6	−4.6 ± 0.3[g]	0.39	−4.0 ± 0.6
Sasebo II	4.3 ± 1.1	4.4 ± 1.0	0.95	0.1 ± 0.5	−0.5 ± 0.3	0.44	−0.3 ± 0.5
Nagasaki	4.6 ± 1.1	3.9 ± 1.0	0.95	−0.6 ± 0.5	−1.0 ± 0.3	0.41	−1.0 ± 0.5
Fukue	2.8 ± 1.0	2.8 ± 0.9	0.96	−0.1 ± 0.5	0.5 ± 0.3	0.32	−0.4 ± 0.5
Kuchinotsu	4.1 ± 1.1	2.9 ± 0.9	0.95	−1.2 ± 0.6	−0.7 ± 0.3	0.42	−1.6 ± 0.6
Akune	3.1 ± 1.0	2.2 ± 0.8	0.95	−0.9 ± 0.5	−0.3 ± 0.3	0.34	−1.2 ± 0.5
Odomari	4.3 ± 1.4	2.8 ± 1.1	0.89	−1.4 ± 0.7	−1.1 ± 0.5	0.22	−1.6 ± 0.7
Nisinoomote	3.4 ± 1.1	3.2 ± 1.2	0.96	−0.2 ± 0.5	−0.3 ± 0.3	0.18	−0.4 ± 0.5
Naha	2.6 ± 1.7	2.7 ± 1.7	0.98	0.2 ± 0.3	0.3 ± 0.2	0.10	0.1 ± 0.3
Mean	4.0 ± 1.4	3.2 ± 1.1	0.97	−0.8 ± 0.3	N/A	0.39	−1.2 ± 0.3

[a] Tide Gauge estimates.
[b] Altimetry estimates.
[c] Correlation between Al and TG.
[d] VLM estimation from SONEL (www.sonel.org) based on altimetry data provided by AVISO at 1° × 1°resolution during 1993–2014.
[e] ICE-6G_C_VM5a model (Stuhne and Peltier, 2015).
[f] Local Land Motion, calculated by VLM minus GIA.
[g] VLM trends from 1993 to 2013.

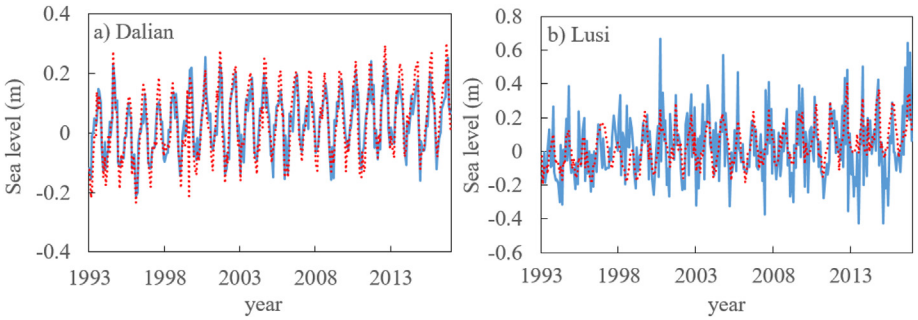

Fig. 3. Comparison of SLC from Altimetry and tide gauge at (a) Dalian and (b) Lusi (the blue straight line is SLC from altimetry and red dot line is from tide gauge). (For interpretation of the references to colour in this figure legend, the reader is referred to the web version of this article.)

Fig. 3 shows a comparison of SLC for Dalian and Lusi from altimetry and tide gauge records during 1993–2016 (see Supplementary Information for other locations). Correlation coefficients between tide gauge and satellite records are higher than 0.75 at all stations except for Lusi (0.55), and most are higher than 0.9. Lusi has both high rates and irregularity in its VLM.

The VLM trends are between −4.5 ± 1.0 and 1.4 ± 1.3 mm/yr. In China, Dalian, Lusi and Kanmen are all subsiding but the VLM rates vary from −3.6 ± 2.6 (Lusi) to −1.3 ± 0.9 (Kanmen) mm/yr. Tsim bei tsui, NPQB and Zhapo are uplifting between 0.7 ± 0.8 and 1.0 ± 1.0 mm/yr. In Korea and Japan, Incheon has an uplifting trend while Mokpo, Jeju, Nagasaki, Kuchinotsu, Akune and Odomari are subsiding. VLM trends have large spatial gradients which contrasts with the slow spatial changes in GIA, suggesting that the VLM variability is mainly due to local land motion. Table 2 also lists the local land motion rate at each station which varies greatly from −5.0 ± 1.0 to 0.8 ± 1.3 mm/yr.

3.2. Sea level trend after removing VLM

Station SLC rates are much higher if VLM is not corrected for. Rates during 1980–2016 range from 2.0 ± 1.5 to 5.7 ± 0.9 mm/yr; Tai po kau, Lusi, Mokpo and Jeju increase at much faster rates than others. Tsim bei tsui, Tai po kau and NPQB stations are all in Hong Kong but their rates have large differences. Assuming that the VLM trend found during 1993–2016 is the same over longer periods, we calculate the sea level trends from the tide gauge stations for two time periods: the whole duration of observations and 1980–2016 (Table 3). After correcting for the VLM, the average SLC rate is 1.8 ± 0.5 mm/yr for the whole duration of observations and 2.9 ± 0.8 mm/yr during 1980–2016.

4. Sea level components

4.1. Steric Sea level

We use spatial correlation between tide gauge record and the gridded steric sea level over the North Pacific to determine the controlling factors for steric signal at the tide gauge locations. Fig. 4 shows an example of the correlations, using the Dalian station. Correlation maps for other stations are shown in the Supplementary Information. Before removing the seasonal cycle, the tide gauge record at Dalian is highly correlated with the steric sea level along the Chinese coast and North Pacific, and the correlation is reduced after removal of the seasonal cycle. Correlations are higher between the tide gauge record and

Table 3
The SLC from tide gauge records (Units: mm/yr) and after correcting for VLM, uncertainties are the 95% confidence interval.

Station	Whole duration			1980–2016	
	Period	Uncorrected	Corrected	Uncorrected	Corrected
Dalian	1970–2016	3.5 ± 0.4	1.8 ± 0.4	3.8 ± 0.5	2.1 ± 0.5
Lusi	1967–2016	5.7 ± 0.4	2.1 ± 0.4	5.0 ± 0.9	1.4 ± 0.9
Kanmen	1959–2016	2.4 ± 0.4	1.1 ± 0.4	3.2 ± 0.7	2.0 ± 0.7
Tsim bei tsui	1974–2016	0.4 ± 1.2	1.5 ± 1.2	2.0 ± 1.5	3.0 ± 1.5
Tai po kau	1963–2016	3.2 ± 0.6	3.2 ± 0.6	5.2 ± 1.1	5.2 ± 1.1
NPQB	1950–2016	1.3 ± 0.5	2.1 ± 0.5	3.1 ± 1.0	4.0 ± 1.0
Zhapo	1959–2016	2.3 ± 0.4	3.0 ± 0.4	3.0 ± 0.7	3.7 ± 0.7
Incheon	1960–2016	1.4 ± 0.5	2.7 ± 0.5	4.0 ± 1.4	5.4 ± 1.4
Mokpo	1960–2016	3.9 ± 0.5	−0.7 ± 0.5	5.7 ± 0.9	1.1 ± 0.9
Jeju	1964–2016	5.3 ± 0.4	1.8 ± 0.4	5.7 ± 0.5	2.1 ± 0.5
Sasebo II	1966–2016	2.2 ± 0.5	2.3 ± 0.5	3.4 ± 0.6	3.5 ± 0.6
Nagasaki	1965–2016	2.6 ± 0.4	2.0 ± 0.4	3.7 ± 0.5	3.1 ± 0.5
Fukue	1965–2016	1.5 ± 0.4	1.4 ± 0.4	2.9 ± 0.5	2.8 ± 0.5
Kuchinotsu	1975–2016	3.3 ± 0.5	2.2 ± 0.5	3.9 ± 0.6	2.7 ± 0.6
Akune	1970–2016	1.4 ± 0.5	0.5 ± 0.5	2.9 ± 0.5	2.0 ± 0.5
Odomari	1965–2016	2.1 ± 0.5	0.6 ± 0.5	3.9 ± 0.7	2.5 ± 0.7
Nisinoomote	1965–2016	2.3 ± 0.4	2.1 ± 0.4	3.1 ± 0.6	2.9 ± 0.6
Naha	1966–2016	2.2 ± 0.6	2.3 ± 0.6	2.5 ± 0.9	2.6 ± 0.9
Mean		2.6 ± 0.5	1.8 ± 0.5	3.7 ± 0.8	2.9 ± 0.8

the upper 700 m steric sea level. Other stations have similar spatial patterns of correlation as Dalian. That is the seasonal cycle is correlated in the Northern Hemisphere and anti-correlated in the Southern Hemisphere, as may be expected from the seasonal patterns of heating. There is a stronger band of seasonal correlation slightly north of the equator along the Pacific that may be related to seasonal precipitation along, and movement of, the Inter Tropical Convergence Zone. Deseasonalized correlations maps show higher correlations around the outer tropics (about 30°N and S), possibly related to the descending branch of the Hadley Circulation where seasonal precipitation effects are minimal.

The largest variations in steric sea level occur due to thermal expansion and contraction of the water column. This variability is driven by heat fluxes and advection of water, and the wind stress (Gill and Niller, 1973; Calafat et al., 2012; Dangendrof et al., 2014). Water exchange is an important contributor to the seasonal cycle of sea level in all China Seas which receive water from the Pacific, and which are affected by turbulent heat fluxes across their surfaces (Ichikawa and Beardsley, 1993; Han and Huang, 2008; Qu et al., 2000, 2004; Rong et al., 2007).

There is almost no contribution of the steric signal at coastal sites as they are relatively very shallow, and calculating local ocean dynamics from the steric sea level signal at the location will not provide reliable spatial information due to boundary dynamics and the presence of fine scale coastal features. Hence here we use the basin-mean steric sea level of the Northwest Pacific (100–140°E, 15–40°N) as a proxy for local steric effects on tide gauges along the Chinese Seas coastline. We calculate the basin-mean steric sea level over 1950–2016. Fig. 5 shows the low-pass filtered monthly full-depth steric sea level and upper 700 m ocean steric sea level in the Northwest Pacific basin. The full-depth steric sea level between 1950 and 2016 increased at the rate of 0.5 ± 0.2 mm/yr while upper 700 m ocean rate was 0.4 ± 0.2 mm/yr. The upper ocean rate was 80% of the full depth rate. During 1980–2016, the full-depth rate increased to 0.8 ± 0.4 mm/yr while

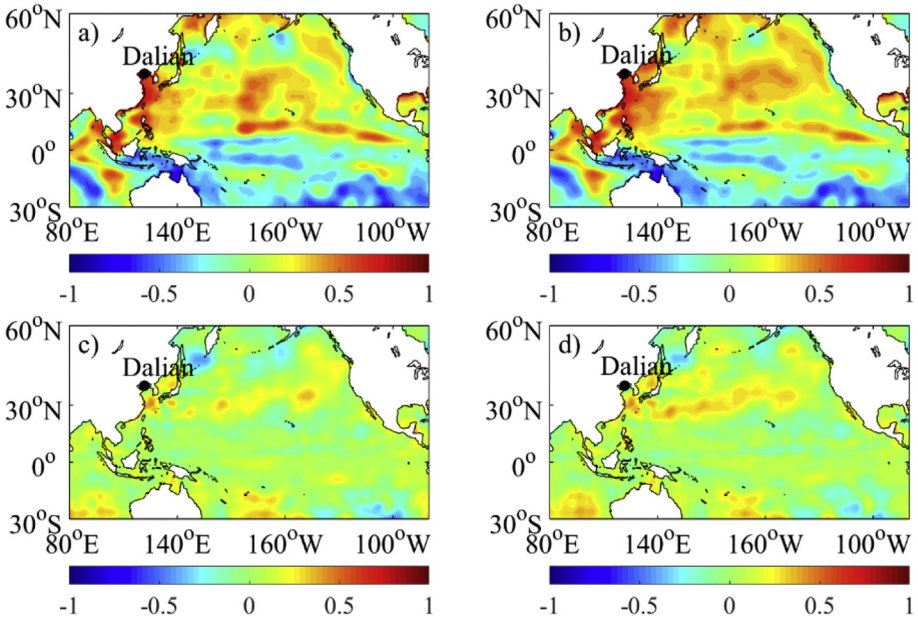

Fig. 4. The correlation between tide gauge record in Dalian and (a) steric sea level for full depth (b) steric sea level for upper 700 m (c) deseasonalized steric sea level for full depth (d) deseasonalized steric sea level for upper 700 m.

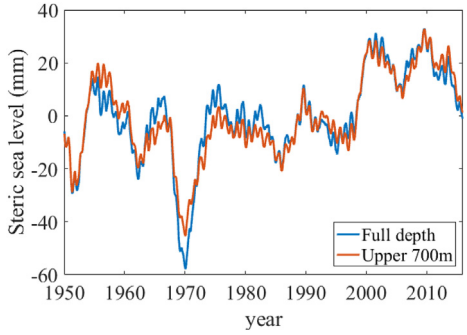

Fig. 5. Low-pass monthly basin-mean steric sea level in the Northwest Pacific basin.

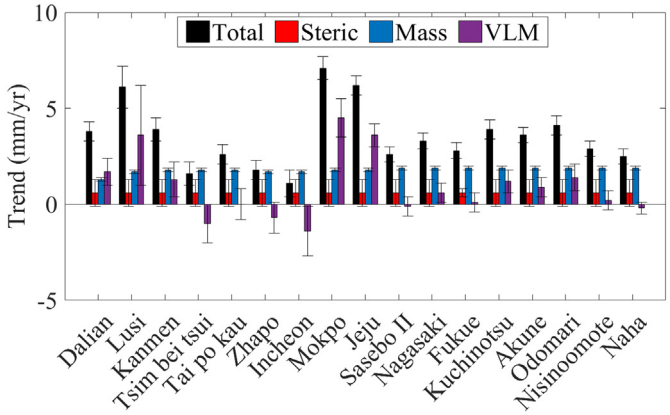

Fig. 6. Total trend of SLC and individual contributors at each location over 1993–2016, uncertainties are the 95% confidence interval.

upper ocean rate increased to 0.9 ± 0.3 mm/yr, 112% of the full depth rate, so increases in steric sea level in the second half of the record were dominated by the upper ocean. According to Ishii et al. (2006), thermal expansion averaged over all longitudes between 60°S and 60°N accounts for almost half of sea level rise during the past decade. Salinity variability contributes much less to the steric sea level change than temperature variability. Thus the increasing rate of steric sea level in the Northwest Pacific basin may be attributed to warming of the upper ocean, characterized by the rises seen in the coastal tide gauge stations we have analyzed.

4.2. Sea level budget

For each tide gauge station during the whole period of observations, we estimate individual contributors as well as their sum. The steric sea level at each station is the basin-mean steric sea level covering the overlapping years with the tide gauge record. For SLC caused by mass change, we use data from Frederikse et al. (2018) covering 1958–2014. Many tide gauge records extend to 2016, so we assume that the annual mass change for 2014–2016 is the same as that for 2013–2014. Stations that start before 1958 are excluded. The VLM trends we use are estimated from altimetry minus tide gauge during 1993–2016, assuming it remains the same for the whole duration of tide gauge records. Table 4 shows the individual contributors (Steric, Mass and VLM) and the sum at each tide gauge station during its whole period.

Steric sea level rises at rates between 0.5 ± 0.2 and 0.9 ± 0.3 mm/yr. The mass change trends are between 0.6 ± 0.1 and 1.1 ± 0.1 mm/yr, and there are no large spatial differences across the region. For most stations, steric and mass change make a similar contribution to sea level rise. There are large differences in the sea level trend contributor of VLM across tide gauge stations, with rates varying from −1.4 ± 1.3 to 4.5 ± 1.0 mm/yr.

For ten stations including Dalian, Lusi, Kanmen, Tsim bei tsui, Jeju, SaseboII, Nagasaki, Fukue, Kuchinotsu, Nisinoomote, the sum of contributors are all close to the trend of tide gauge records and the differences are within ± 0.6 mm/yr. But for some others there are large differences. The failure to close the sea level budget for each tide gauge station over the whole observational period is due to the underestimation or overestimation of contributors, most likely VLM. This because we assume the VLM trends estimated from satellite altimetry minus tide gauge remain the same for the whole duration of tide gauge records and VLM trends have much larger uncertainties than do steric and mass trends in most stations. For Dalian, Lusi, Kanmen and Jeju, the contribution of VLM is much higher than steric and present-day mass redistribution, and the fast rate of land subsidence is the main cause of sea level rise.

Also we estimate the sea level budget for each tide gauge location over 1993–2016 and it is shown in Fig. 6. During 1993–2016, for Dalian, Lusi, Mokpo and Jeju, VLM is the main contributor to sea level rise; while for Kanmen, Tsim bei tsui, Tai po kau, Zhapo, Incheon, Sasebo II, Nagasaki, Fukue, Kuchinotsu, Akune, Odomari, Nisinoomote and Naha, mass loss is the main source of sea level rise, the steric sea level component has largest uncertainty. This is not due to random

Table 4
Sea level trend of contributors and their sum (mm/yr), uncertainties are the 95% confidence interval.

	Time span of record	Sea level contributors			Sum of contributors	Tide gauge record
		Steric	Mass	VLM		
Dalian	1970–2016	0.7 ± 0.3	0.6 ± 0.1	1.7 ± 0.7	3.0 ± 0.4	3.5 ± 0.4
Lusi	1967–2016	0.9 ± 0.3	0.8 ± 0.1	3.6 ± 2.6	5.3 ± 1.0	5.7 ± 0.4
Kanmen	1959–2016	0.6 ± 0.2	0.7 ± 0.1	1.3 ± 0.9	2.6 ± 0.4	2.4 ± 0.4
Tsim bei tsui	1974–2016	0.7 ± 0.3	1.0 ± 0.1	−1.0 ± 1.0	0.7 ± 0.5	0.4 ± 1.2
Tai po kau	1963–2016	0.7 ± 0.2	0.8 ± 0.1	0.0 ± 0.8	1.5 ± 0.4	3.2 ± 0.6
NPQB	1950–2016	0.5 ± 0.2	N/A	−0.9 ± 0.7	N/A	1.3 ± 0.5
Zhapo	1959–2016	0.6 ± 0.2	0.7 ± 0.1	−0.7 ± 0.8	0.6 ± 0.4	2.3 ± 0.4
Incheon	1960–2016	0.7 ± 0.2	0.7 ± 0.1	−1.4 ± 1.3	0.0 ± 0.5	1.4 ± 0.5
Mokpo	1960–2016	0.7 ± 0.2	0.7 ± 0.1	4.5 ± 1.0	5.9 ± 0.4	3.9 ± 0.5
Jeju	1964–2016	0.7 ± 0.3	0.8 ± 0.1	3.6 ± 0.6	5.1 ± 0.3	5.3 ± 0.4
Sasebo II	1966–2016	0.9 ± 0.3	0.8 ± 0.1	−0.1 ± 0.5	1.6 ± 0.3	2.2 ± 0.5
Nagasaki	1965–2016	0.8 ± 0.3	0.8 ± 0.1	0.6 ± 0.5	2.2 ± 0.3	2.6 ± 0.4
Fukue	1965–2016	0.8 ± 0.3	0.8 ± 0.1	0.1 ± 0.5	1.7 ± 0.3	1.5 ± 0.4
Kuchinotsu	1975–2016	0.7 ± 0.3	1.1 ± 0.1	1.2 ± 0.6	3.0 ± 0.3	3.3 ± 0.5
Akune	1970–2016	0.7 ± 0.3	1.0 ± 0.1	0.9 ± 0.5	2.5 ± 0.3	1.4 ± 0.5
Odomari	1965–2016	0.8 ± 0.3	0.8 ± 0.1	1.4 ± 0.7	3.1 ± 0.4	2.1 ± 0.5
Nisinoomote	1965–2016	0.8 ± 0.3	0.8 ± 0.1	0.2 ± 0.5	1.8 ± 0.3	2.3 ± 0.4
Naha	1966–2016	0.9 ± 0.3	0.9 ± 0.1	−0.2 ± 0.3	1.6 ± 0.2	2.2 ± 0.6

Table 5
Sea level projection at 2100 relative to 1986–2005 for 5%, 50% and 95% probability at each station (Units: cm).

Station	RCP 4.5			High-end RCP 8.5		
	5	50	95	5	50	95
Dalian	33	51	69	50	88	185
Qinhuangdao	32	48	64	48	84	177
Yantai	33	51	69	50	88	185
Lusi	35	52	68	50	88	187
Kanmen	39	57	75	54	95	198
Keelung II	40	58	76	55	95	199
Xiamen	36	55	73	51	92	194
Macau	38	56	73	53	92	192
Tsim bei tsui	38	56	73	53	92	192
Tai po kau	38	56	73	53	92	192
NPQB	38	56	73	53	92	192
Chi ma wan	38	56	73	53	92	192
Zhapo	40	57	74	54	93	194
Incheon	35	53	72	51	90	192
Mokpo	35	53	72	51	90	192
Jeju	36	55	74	52	92	195
Sasebo II	37	55	73	53	93	195
Nagasaki	37	55	73	53	93	195
Fukue	37	55	73	54	93	196
Kuchinotsu	37	55	73	53	93	196
Akune	40	59	77	56	98	202
Odomari	39	59	78	56	98	203
Nisinoomote	39	59	78	56	98	203
Naha	42	61	80	57	99	205
Hondau	37	54	70	51	89	188
Mean	37	55	73	53	92	194

noise in steric sea level but from autocorrelated processes that are not accounted for by a simple linear fit to the time series (e.g. Fig. 5).

5. Sea level projection

We show median (50%) and 5 and 95% of sea level rise by 2100 under the RCP 4.5 and High-end RCP 8.5 scenarios relative to 1986–2005 for the 25 stations (Table 5). Fig. 7 shows projections for sea level components and total sea level at Dalian as an example. Steric SLC is the main source of sea level rise under both scenarios with the Glaciers contribution second, then comes the contributions from GIS and AIS. Land-water storage makes little contribution. GIA makes negative contributions to future sea level rise. For Dalian, sea level projected rises are > 0.4 m by 2100 under the RCP 4.5 scenario and > 0.8 m under the High-end RCP 8.5 scenario. The sea level projections for other stations are quite similar to Dalian. Fig. 8(a)–(f) are the projection averaged over 25 stations at different probabilities, and shows that under both scenarios, the steric effect is the main source of sea level rise at all probabilities except at the high projection tail of the High-end RCP 8.5 scenario, when the AIS makes more than half the total contribution.

From Table 5 we can see for RCP 4.5 all station projections at 5%, 50% and 95% levels at 2100 are [32 42] cm, [48 61] cm and [64 80] cm respectively. For High-end RCP 8.5 scenario, the projections are [48 57] cm, [84 99] cm and [177205] cm respectively. Qinhuangdao has the lowest sea level projections for all scenarios while Naha has the highest. Under both scenarios, stations in Korea and Japan have higher projections than China; stations in Taiwan, Southern China and Eastern China have higher projections than Northern China.

Future sea level projection are made at ten-year time steps, so seasonal and annual cycles are not included. Monthly tide gauge observations record such variability and it is important for future sea level projections. We illustrate this effect by connecting the tide gauge record after removing VLM with future sea level projections: Fig. 9 shows Dalian, other stations are in the Supplementary Information. Future decadal sea level projections during 2010–2100 were linearly interpolated onto annual time steps.

6. Discussion

6.1. Comparison with previous studies

Chen et al. (2018) used 10 tide gauge records to study the mean relative sea level rise along the coastline of the China Seas and found it increases at the rates from 1 to 5 mm/yr from the mid-20st century. We calculated VLM from altimetry minus tide gauge records. The consistency of the satellite altimetry and tide gauge indicates the good quality of the high-resolution AVISO data. Large spatial differences exist and the VLM trend varies from -4.5 ± 1.0 mm/yr to 1.4 ± 1.3 mm/yr. The stations along the South China Sea have an uplifting trend as a whole. The subsidence of mainland China stations is largely due to over-extraction of groundwater since the 1990s for the rapidly developing coastal cities (Chen, 1997). Lusi subsides at the fastest rate (-3.6 ± 2.6 mm/yr), which contributes to the increasing SLC trend of its tide gauge. Lusi is in Nantong City on the Yangtze River Delta, and water from depths of 300-400 m are being extracted, which together with the sandy local environment causes severe subsidence in this area (Ren, 1993).

We use VLM calculated from high-resolution altimetry datasets that are within the 95% confidence intervals of estimates from SONEL (www.sonel.org). The differences between VLM trends estimated in this paper and SONEL come from the different altimetry products used. Chen et al. (2018) also estimated the VLM trend using 10 tide gauge stations over 1993–2012 with the same method, and the results were consistent with our study. Chen et al. (2018) also compared this VLM estimation with the few available GPS estimates which have smaller uncertainties.

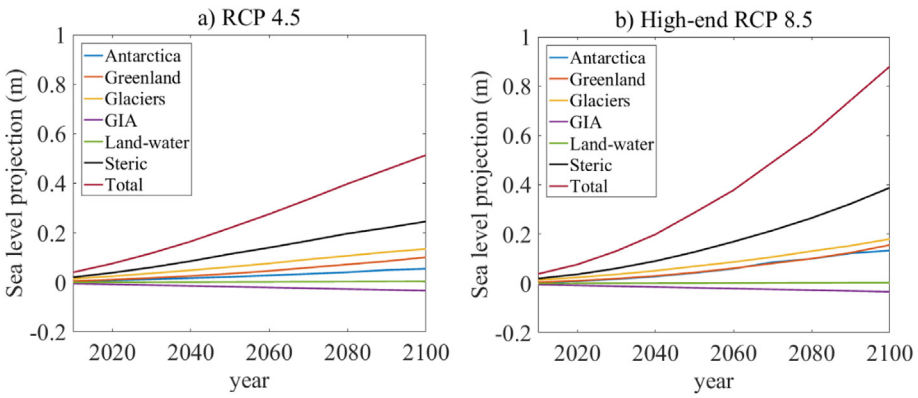

Fig. 7. Future median (50%) sea level projection for Dalian under RCP 4.5 and High-end RCP 8.5 scenarios relative to 1986–2005.

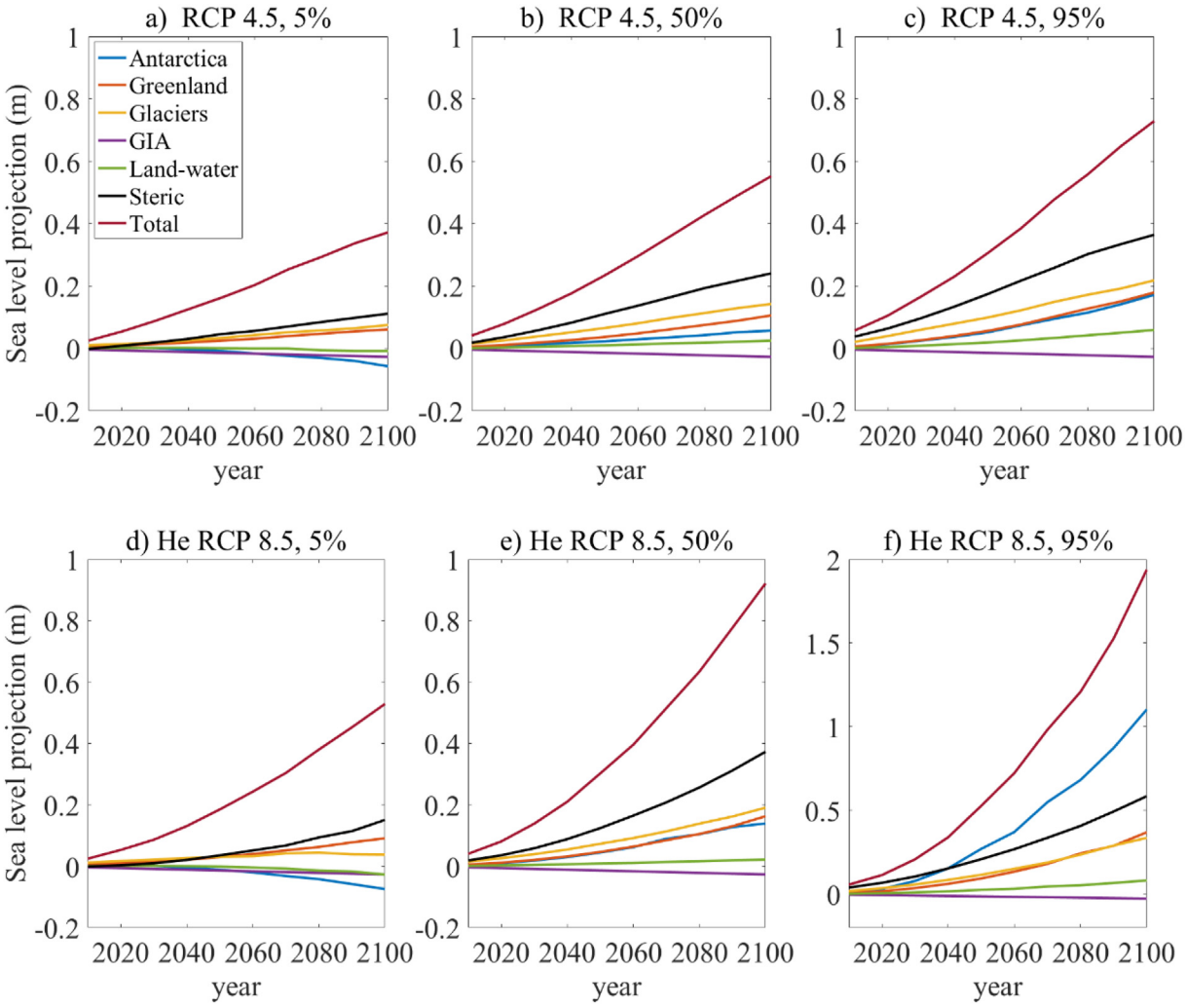

Fig. 8. Future sea level projection averaged over 25 stations for 5%, 50% and 95% probability respectively under RCP 4.5 and High-end RCP 8.5 scenarios relative to 1986–2005.

6.2. Uncertainties in future sea level projection

There are large uncertainties in future sea level projections with the RCP 4.5 and High-end RCP 8.5 scenarios associated with emissions scenarios, outputs from CMIP5 models, estimates of ice mass lost from ice sheets in Greenland and Antarctica and GIA corrections, which have been widely discussed in previous studies (Church et al., 2013; Kopp et al., 2014; Jackson and Jevrejeva, 2016; Jevrejeva et al., 2016; Chen et al., 2018). In our study sea level budgets calculated for individual tide gauges locations provide evidence of large contributions (up to 5.0 ± 1.0 mm/yr) to sea level rise from local vertical land movement over the past 24 years. However, it is difficult to estimate future changes in local vertical land movement and in this study we only project changes due to GIA. For example, if the VLM in future keeps the same rate as that over 1993–2016, i.e., assuming Lusi keeps subsiding at 4.1 mm/yr, then sea level will rise by about 40 cm more than the projection by the end of 2100.

If the coastal cities with large subsidence keep subsiding then they will be much more vulnerable to future sea level rise than we ever thought (Jevrejeva et al., 2016). Lack of GPS data in tide gauge locations is limiting our interpretation of past sea level records and introducing additional uncertainties in future sea level projections.

The seasonal amplitude should be taken into consideration in future sea level projection as it is also of vital importance for coastal defense. In future we are aiming to estimate uncertainties due to seasonal and interannual variability in coastal sea level, which is currently not represented in outputs from CMIP5 models.

7. Conclusions

Due to the limited tide gauge records and GPS data, previous studies are unable to explain the sea level budgets along the China Seas, most papers have focused on the sea level change at a few stations. In our study, we made use of 25 tide gauge records lining the China Seas. We analyzed the sea level rise, estimating local land movement. We calculated the contributions from steric and mass changes to estimate the sea level budget of each station. Finally we made projections of future sea level for each station unde the RCP 4.5 and High-end RCP 8.5 scenarios.

The analysis of sea level trends show that during their whole observational periods, the sea levels of 25 tide gauge stations along the China Seas coast change at rates between −2.3 ± 1.9 and 5.7 ± 0.4 mm/yr. Three stations show a falling trend and 22 stations show an increasing trend and the rates of increase vary greatly. As there are large spatial differences in the trend of SLC which cannot be explained by GIA, this difference is related to local land-motion. For China, only limited and short GPS data are available, and we estimated the VLM from satelite altimetry and the tide gauges from 1993 to 2016. VLM varies considerably while GIA are quite similar, hence local land-motion accounts for the large differences. After removing the VLM

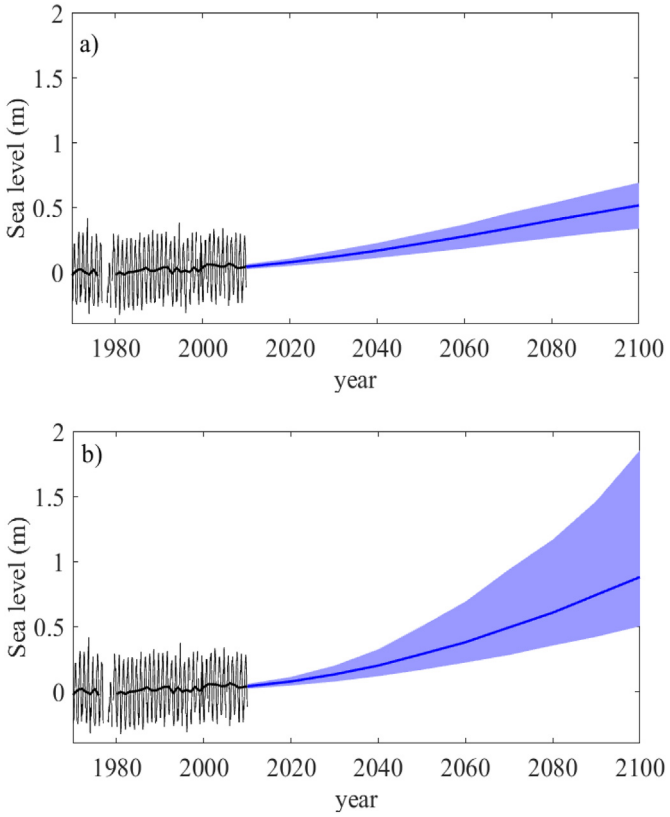

Fig. 9. Tide gauge observations (black lines) combined with sea level projections (blue) under (a) RCP 4.5 and (b) High-end RCP 8.5 scenarios at Dalian (The thin black line is monthly tide gauge record, the thick black line is annual tide gauge record; the thick blue line is sea level projection at 50% probability, for the blue shading area is 5–95%). (For interpretation of the references to colour in this figure legend, the reader is referred to the web version of this article.)

trend, the mean SLC trend demonstrate: (1) Since the 1950s, coastal sea level rises at the rate of 1.8 ± 0.5 mm/yr; (2) During 1980–2016, sea level is rising at the rate of 2.9 ± 0.8 mm/yr; (3) During 1993–2016, it rises at the rate of 3.2 ± 1.1 mm/yr.

The correlation between tide gauge records and steric sea level in the North Pacific before and after removing seasonal cycle was used to examine the seasonal cycle in sea levels and determine the source of steric signal at tide gauge locations. The high correlation between tide gauge record and steric sea level along the China Seas coast and North Pacific is dominated by the seasonal cycle, and the correlation is higher between tide gauge record and upper ocean steric sea level.

We used the basin-mean steric sea level of the Northwest Pacific as a proxy for the local steric effects on tide gauge station with the present-day mass redistribution estimated by Frederikse et al. (2018), and the VLM trend calculated from altimetry minus tide gauge. We estimate the contributions including steric, mass change and VLM to each tide gauge records over the whole observational period, steric sea level contributes up to 0.9 ± 0.3 mm/yr, and ice mass loss from glaciers and ice sheets contributes up to 1.1 ± 0.1 mm/yr over the last 60 years. Contribution from VLM ranges between −4.5 ± 1.0 mm/yr and 1.4 ± 1.3 mm/yr across stations.

Finally, we made sea level projections with individual contributors for each station under RCP 4.5 and High-end RCP 8.5 scenarios. Projected sea level shows an increasing trend for all stations over 2010–2100 with the steric effect as the main contributor under RCP 4.5 and High-end RCP 8.5 scenarios except at 95% high end projection for High-end, RCP 8.5 when the Antarctic ice sheet makes the main contribution.

Acknowledgements

Tide gauge data are obtained from the Permanent Service for Mean Sea level (PSMSL) (www.psmsl.org). EN4 version 4.2.0 gridded temperature and salinity data are obtained from the U.K. Met Office (www.metoffice.gov.uk/hadobs/en4/). Altimetry data provided by SSALTO/DUACS are obtained from AVISO (www.aviso.altimetry.fr). Sea level pressure are downloaded from NCEP/NCAR Reanalysis datasets (www.esrl.noaa.gov/psd). GH thanks Thomas Frederikse for providing the present-day mass redistribution data, and Francisco Mir. Calafat for the helpful suggestions. Also the authors gratefully acknowledge the financial support from China Scholarship Council. SJ was supported by the Natural Environmental Research Council under Grant Agreement No. NE/P01517/1 for the project called “Sea level rise trajectories by 2200 with warmings of 1.5 to 2 °C" and by the EPSRC NEWTON Fund Sustainable Deltas Programme, grant number EP/R024537/1, ANCODE project (Applying nature-based coastal defense to the world's largest urban area – from science to practice).

Appendix A. Supplementary data

Supplementary data to this article can be found online at https://doi.org/10.1016/j.gloplacha.2018.11.005.

References

Bamber, J.L., Aspinall, W.P., 2013. An expert judgement assessment of future sea level rise from the ice sheets. Nat. Clim. Chang. 3, 424–427. https://doi.org/10.1038/NCLIMATE1778.

Bamber, J., Riva, R., 2010. The sea level fingerprint of recent ice mass fluxes. Cryosphere 4, 621–627. https://doi.org/10.5194/tc-4-621-2010.

Calafat, F.M., Chambers, D.P., Tsimplis, M.N., 2012. Mechanisms of decadal sea level variability in the eastern North Atlantic and the Mediterranean Sea. J. Geophys. Res. 117, C09022. https://doi.org/10.1029/2012JC008285.

Chen, X.Q., 1991. Sea level changes since the early 1920's from the long records of two tidal gauges in Shanghai. China J. Coast. Res. 7 (3), 787–799. http://www.jstor.org/stable/4297894.

Chen, J., 1997. The impact of Sea level rise on China's Coastal areas and its disaster Hazard Evaluation. J. Coast. Res. 2050, 925–930.

Chen, N., Han, G., Yang, J., 2018. Mean relative sea level rise along the coasts of the China Seas from mid-20th to 21st centuries. Cont. Shelf Res. 152, 27–34. https://doi.org/10.1016/j.csr.2017.12.002.

China Sea Level Bulletin of 2016, 2017. State Oceanic Administration. http://www.soa.gov.cn.

Church, J.A., et al., 2013. Sea level change. In: Stocker, T.F., Qin, D., Plattner, G.-K., Tignor, M., Allen, S.K., Boschung, J., Nauels, A., Xia, Y., Bex, V., Midgley, P.M. (Eds.), Climate Change 2013: The Physical Science Basis. Contribution of Working Group I to the Fifth Assessment Report of the Intergovernmental Panel on Climate Change. Cambridge University Press, Cambridge and New York.

Dangendrof, S., Calafat, F.M., Arns, A., Wahl, T., Haigh, I.D., Jensen, J., 2014. Mean sea level variability in the North Sea: processes and implications. J. Geophys. Res. Oceans. (2), 1022–1037. https://doi.org/10.1002/2013JC009415.

Ding, X., Zheng, D., Chen, Y., Chao, J., Li, Z., 2001. Sea level change in Hong Kong from tide gauge measurements of 1954–1999. J. Geod. 74, 683–689. https://doi.org/10.1007/s001900000128.

Emery, K.O., Yu, F.H., 1981. Sea level changes in the Western Pacific with emphasis on China. Oceanologia et Limnologia Sinica. 12 (4), 297–310.

Frederikse, T., Jevrejeva, S., Riva, R.E.M., Dangendorf, S., 2018. A consistent sea-level reconstruction and its budget on basin and global scales over 1958–2014. J. Clim. 31 (3), 1267–1280. https://doi.org/10.1175/JCLI-D-17-0502.1.

Gill, A.E., Niller, P.P., 1973. The theory of the seasonal variability in the ocean. Deep-Sea Res. Oceanogr Abstracts 20 (2), 141–177. https://doi.org/10.1016/0011-7471(73)90049-1.

Good, S.A., Martin, M.J., Rayner, N.A., 2013. EN4: quality controlled ocean temperature and salinity profiles and monthly objective analyses with uncertainty estimates. J. Geophys. Res. Oceans. 118, 6704–6716. https://doi.org/10.1002/2013JC009067.

Gouretski, V., Reseghetti, F., 2010. On depth and temperature biases in bathythermograph data: development of a new correction scheme based on analysis of a global ocean database. Deep-Sea Res. I 57 (6). https://doi.org/10.1016/j.dsr.2010.03.011.

Grinsted, A., Jevrejeva, S., Riva, R.E.M., Dahl-Jensen, D., 2015. Sea level rise projections for northern Europe under RCP8.5. Clim. Res. 64, 15–23. https://doi.org/10.3354/cr01309.

Hallegatte, S., Green, C., Nicholls, R.J., Corfee-Morlot, J., 2013. Future flood losses in major coastal cities. Nat. Clim. Chang. 3, 802–806. https://doi.org/10.1038/NCLIMATE1979.

Han, G., Huang, W., 2008. Pacific Decadal Oscillation and Sea Level Variability in the Bohai, Yellow, and East China Seas. J. Phys. Oceanogr. 38 (12), 2772–2783. https://

doi.org/10.1175/2008JPO3885.1.
Han, M., Hou, J., Wu, L., 1995. Potential impacts of Sea level rise on China's coastal environment and cities: a national assessment. J. Coast. Res. (14), 79–95.
He, L., Li, G.S., Li, K., Shu, Y.Q., 2014. Estimation of regional sea level change in the Pearl River Delta from tide gauge and satellite altimetry data. Estuar. Coast. Shelf Sci. 141, 69–77. https://doi.org/10.1016/j.ecss.2014.02.005.
Holgate, S.J., Matthews, A., Woodworth, P.L., Rickards, L.J., Tamisiea, M.E., Bradshaw, E., Foden, P.R., Gordon, K.M., Jevrejeva, S., Pugh, J., 2013. New data systems and products at the permanent service for mean sea level. J. Coast. Res. 29 (3), 493–504. https://doi.org/10.2112/JCOASTRES-D-12-00175.1.
Ichikawa, Hiroshi, Beardsley, R.C., 1993. Temporal and spatial variability of volume transport of the Kuroshio in the East China Sea. Deep-Sea Res. Part I: Oceanogr. Res. Pap. 40 (3), 583–605. https://doi.org/10.1016/0967-0637(93)90147-U.
Ishii, M., Kimoto, M., Sakamoto, K., Iwasaki, S.I., 2006. Steric Sea level changes estimated from historical ocean subsurface temperature and salinity analyses. J. Oceanogr. 62 (2), 155–170. https://doi.org/10.1007/s10872-006-0041-y.
Jackson, L.P., Jevrejeva, S., 2016. A probabilistic approach to 21st century regional sea level projections using RCP and high-end scenarios. Glob. Planet. Change 146, 179–189. https://doi.org/10.1016/j.gloplacha.2016.10.006.
Jevrejeva, S., Grinsted, A., Moore, J.C., 2014. Upper limit for Sea level projections by 2100. Environ. Res. Lett. 9. https://doi.org/10.1088/1748-9326/9/10/104008.
Jevrejeva, S., Jackson, L.P., Riva, R.E.M., Grinsted, A., Moore, J.C., 2016. Coastal Sea level rise with warming above 2 °C. Proc. Natl. Acad. Sci. 113 (47), 13342–13347. https://doi.org/10.1073/pnas.1605312113.
Kalnay, E., et al., 1996. The NCEP/NCAR 40-year reanalysis project. Bull. Am. Meteor. Soc. 77, 437–470.
Kjeldsen, K.K., Korsgaard, N.J., Bjørk, A.A., Khan, S.A., Box, J.E., Funder, S., Larsen, N.K., Bamber, J.L., Colgan, W., Broeke, M.V.D., Andersen, M.L.S., Nuth, C., Schomacker, A., Andresen, C.S., Willerslev, E., Kjær, K.H., 2015. Spatial and temporal distribution of mass loss from the Greenland Ice Sheet since AD 1900. Nature 528 (7582), 396–400. https://doi.org/10.1038/nature16183.
Kleinherenbrink, M., Riva, R., Frederikse, T., 2018. A comparison of methods to estimate vertical land motion trends from GNSS and altimetry at tide gauge stations. Ocean Sci. 14, 187–204. https://doi.org/10.5194/os-14-187-2018.
Kopp, R.E., Horton, R.M., Little, C.M., Mitrovica, J.X., Oppenheimer, M., Rasmussen, D.J., Strauss, B.H., Tebaldi, C., 2014. Probabilistic 21st and 22nd century Sea level projections at a global network of tide-gauge sites. Earth's Future 383–406. https://doi.org/10.1002/2014EF000239.
Kuo, C.Y., Shum, C.K., Braun, A., Mitrovica, J.X., 2004. Vertical crustal motion determined by satellite altimetry and tide gauge data in Fennoscandia. Geophys. Res. Lett. 31 (1), 1–4. https://doi.org/10.1029/2003GL019106.
Marzeion, B., Leclercq, P.W., Cogley, J.G., Jarosch, A.H., 2015. Brief communication: global reconstructions of glacier mass change during the 20th century are consistent. Cryosphere 9 (6), 2399–2404. https://doi.org/10.5194/tc-9-2399-2015.
McDougall, T.J., Barker, P.M., 2011. Getting started with TEOS-10 and the Gibbs Seawater (GSW) oceanographic toolbox. SCOR/IAPSO WG. Vol. 127. pp. 1–28.
Moss, R.H., Edmonds, J.A., Hibbard, K.A., Manning, M.R., Rose, S.K., Vuuren, D.P.V., Carter, T.R., Emori, S., Kainuma, M., Kram, T., Meehl, G.A., Mitchell, J.F.B., Nakićenović, N., Riahi, K., Smith, S.J., Stouffer, R.J., Thomson, A.M., Weyant, J.P., Wilibanks, T.J., 2010. The next generation of scenarios for climate change research and assessment. Nature 463, 747–756. https://doi.org/10.1038/nature08823.
Ostanciaux, É., Husson, L., Choblet, G., Robin, C., Pedoja, K., 2012. Present-day trends of vertical ground motion along the coast lines. Earth-Sci. Rev. 110 (1–4), 74–92. https://doi.org/10.1016/j.earscirev.2011.10.004.
Peltier, W.R., Argus, D.F., Drummond, R., 2015. Space geodesy constrains ICE age terminal deglaciation: the global ICE-6G C (VM5a) model. J. Geophys. Res. Solid Earth 119. https://doi.org/10.1002/2014JB011176.
Permanent Service for Mean Sea level (PSMSL), 2017. Tide Gauge Data (Retrieved 09 Oct 2017 from). http://www.psmsl.org/data/obtaining/.
Prandi, P., Cazenave, A., Becker, M., 2009. Is coastal mean sea level rising faster than the global mean? A comparison between tide gauges and satellite altimetry over 1993–2007. Geophys. Res. Lett. 36, L05602. https://doi.org/10.1029/2008GL036564.
Qu, T., Mitsudera, H., Yamagata, T., 2000. Intrusion of the North Pacifica waters into the South China Sea. J. Geophys. Res. 105, 6415–6424. https://doi.org/10.1029/1999JC900323.
Qu, T., Kim, Y.Y., Yaremchuk, M., Tozuka, T., Ishida, A., Yamagata, T., 2004. Can Luzon strait transport play a role in conveying the impact of ENSO to the South China Sea? J. Clim. 17, 3644–3657. https://doi.org/10.1175/1520-0442(2004)017<3644:CLSTPA>2.0.CO;2.
Ren, M.E., 1993. Relative Sea level changes in China over the last 80 years. J. Coast. Res. 9 (1), 229–241. http://www.jstor.org/stable/4298080.
Rong, Z., Liu, Y., Zong, H., Cheng, Y., 2007. Interannual Sea level variability in the South China Sea and its response to ENSO. Glob. Planet. Chang. 55 (4), 257–272. https://doi.org/10.1016/j.gloplacha.2006.08.001.
Rowley, R.J., Kostelnick, J.C., Braaten, D., Li, X., Meisel, J., 2007. Risk of rising sea level to population and land area. EOS Trans. Am. Geophys. Union 88 (9), 105–116. https://doi.org/10.1029/2007EO090001.
Shi, Y.F., Zhu, J.W., Xie, Z.R., Ji, Z.X., Jiang, Z.X., Yang, G.S., 2000. Prediction and prevention of the impacts of sea level rise on the Yangtze River Delta and its adjacent areas. Sci. China (Ser. D) 43 (4), 412–422.
Stuhne, G.R., Peltier, W.R., 2015. Reconciling the ICE-6G_C reconstruction of glacial chronology with ice sheet dynamics: the cases of Greenland and Antarctica. J. Geophys. Res. Earth Surf. 120, 1–25. https://doi.org/10.1002/2015JF003580.
Wada, Y., Beek, L.P.H.V., Weiland, F.C.S., Chao, B.F., Wu, Y.H., Bierkens, M.F.P., 2012. Past and future contribution of global groundwater depletion to sea level rise. Geophys. Res. Lett. 39, L09402. https://doi.org/10.1029/2012GL051230.
Wada, Y., Wisser, D., Bierkens, M.F.P., 2014. Global modeling of withdrawal, allocation and consumptive use of surface water and groundwater resources. Earth Syst. Dyn. 5, 15–40. https://doi.org/10.5194/esd-5-15-2014.
Wang, J., Gao, W., Xu, S.Y., Yu, L.Z., 2012. Evaluation of the combined risk of sea level rise, land subsidence, and storm surges on the coastal areas of Shanghai, China. Clim. Chang. 115 (3–4), 537–558. https://doi.org/10.1007/s10584-012-0468-7.
Wang, L., Huang, G., Zhou, W., Chen, W., 2016. Historical change and future scenarios of sea level rise in Macau and adjacent waters. Adv. Atmos. Sci. 33, 462–475. https://doi.org/10.1007/s00376-015-5047-1.
Warrick, R.A., Ye, W., Kouwenhoven, P., Hay, J.E., Cheatham, C., 2005. New developments of the SimCLIM model for simulating adaptation to risks arising from climate variability and change. In: Zerger, A., ARGENT, R.M. (Eds.), Proceedings of the International Congress on Modelling and Simulation, Modelling and Simulation Society of Australia and New Zealand, Canberra, pp. 170–176.
Wöppelmann, G., Marcos, M., 2016. Vertical land motion as a key to understanding sea level change and variability. Rev. Geophys. 54, 64–92. https://doi.org/10.1002/2015RG000502.
Wu, Q., Zheng, X., Xu, H., Ying, Y., Hou, Y., Xie, X., Wang, S., 2003. Relative Sea-level rising and its control strategy in coastal regions of China in the 21st century. Sci. China Ser. D 46, 74–83.